A new semi-orthotopic bone defect model for cell and biomaterial testing in regenerative medicine

Andrés Sastre, E.; Nossin, Y.; Jansen, I.; Kops, N.; Intini, C.; Witte-Bouma, J.; van Rietbergen, B.; Hofmann, S.; van Osch, G. J.V.M.; More Authors

DOI
10.1016/j.biomaterials.2021.121187

Publication date
2021

Document Version
Final published version

Published in
Biomaterials

Citation (APA)
Andrés Sastre, E., Nossin, Y., Jansen, I., Kops, N., Intini, C., Witte-Bouma, J., van Rietbergen, B., Hofmann, S., van Osch, G. J. V. M., & More Authors (2021). A new semi-orthotopic bone defect model for cell and biomaterial testing in regenerative medicine. *Biomaterials*, *279*, Article 121187. https://doi.org/10.1016/j.biomaterials.2021.121187

Biomaterials 279 (2021) 121187

Contents lists available at ScienceDirect

Biomaterials

journal homepage: www.elsevier.com/locate/biomaterials

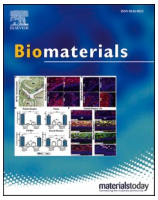

A new semi-orthotopic bone defect model for cell and biomaterial testing in regenerative medicine

E. Andrés Sastre [a], Y. Nossin [b], I. Jansen [a,c,d], N. Kops [e], C. Intini [f], J. Witte-Bouma [a], B. van Rietbergen [c,g], S. Hofmann [c,d], Y. Ridwan [h,i], J.P. Gleeson [f], F.J. O'Brien [f,j,k], E. B. Wolvius [a], G.J.V.M. van Osch [b,e,l,1], E. Farrell [a,*,1]

[a] Department of Oral and Maxillofacial Surgery, Erasmus University Medical Center, Rotterdam, the Netherlands
[b] Department of Otorhinolaryngology, Erasmus University Medical Center, Rotterdam, the Netherlands
[c] Orthopaedic Biomechanics, Department of Biomedical Engineering, Eindhoven University of Technology, Eindhoven, the Netherlands
[d] Institute for Complex Molecular Systems, Department of Biomedical Engineering, Eindhoven University of Technology, Eindhoven, the Netherlands
[e] Department of Orthopaedics and Sports Medicine, Erasmus University Medical Center, Rotterdam, the Netherlands
[f] Tissue Engineering Research Group, Department of Anatomy and Regenerative Medicine, Royal College of Surgeons in Ireland, Dublin, Ireland
[g] Department of Orthopaedic Surgery, Research School CAPHRI, Maastricht University Medical Center, Maastricht, the Netherlands
[h] Department of Molecular Genetics, Erasmus University Medical Center, Rotterdam, the Netherlands
[i] Department of Radiology and Nuclear Medicine, Erasmus University Medical Center, Rotterdam, the Netherlands
[j] SFI Advanced Materials and Bioengineering Research (AMBER) Center, Royal College of Surgeons in Ireland and Trinity College Dublin, Dublin, Ireland
[k] Trinity Center for Biomedical Engineering, Trinity College Dublin, Dublin, Ireland
[l] Department of Biomechanical Engineering, Faculty of Mechanical, Maritime, and Materials Engineering, Delft University of Technology, Delft, the Netherlands

ARTICLE INFO

Keywords:
Animal model
Guided tissue regeneration
Bone
Bone substitutes
Endochondral ossification
Tissue scaffolds

ABSTRACT

In recent decades, an increasing number of tissue engineered bone grafts have been developed. However, expensive and laborious screenings *in vivo* are necessary to assess the safety and efficacy of their formulations. Rodents are the first choice for initial *in vivo* screens but their size limits the dimensions and number of the bone grafts that can be tested in orthotopic locations. Here, we report the development of a refined murine subcutaneous model for semi-orthotopic bone formation that allows the testing of up to four grafts per mouse one order of magnitude greater in volume than currently possible in mice. Crucially, these defects are also "critical size" and unable to heal within the timeframe of the study without intervention. The model is based on four bovine bone implants, ring-shaped, where the bone healing potential of distinct grafts can be evaluated *in vivo*. In this study we demonstrate that promotion and prevention of ossification can be assessed in our model. For this, we used a semi-automatic algorithm for longitudinal micro-CT image registration followed by histological analyses. Taken together, our data supports that this model is suitable as a platform for the real-time screening of bone formation, and provides the possibility to study bone resorption, osseointegration and vascularisation.

1. Introduction

Bone has the ability to heal in most cases with minimal or no scar formation. However, after severe trauma or tumour resection surgery, bone might be unable to heal spontaneously in a reasonable amount of time. Above a critical size, bone defects exhaust their self-healing capacity. In these circumstances, there are many possibilities for intervention that use various grafts to support and promote the regeneration of the bone in the defects [1]. The use of autologous bone as a grafting material is the most successful method to achieve bone augmentation of defects. This strategy constitutes the current gold-standard, as autologous grafts are both osteoinductive and osteoconductive and have a low risk of immune rejection [2]. However, their use is limited to the available amount of harvestable material and often results in donor site morbidity. An alternative approach is to use tissue engineered grafts capable of promoting the bone healing response. In general, these grafts are based on a scaffold that may be combined with either pro-osteogenic agents, such as bone morphogenetic proteins (BMPs), stem cells, other

* Corresponding author.
E-mail address: e.farrell@erasmusmc.nl (E. Farrell).
[1] These authors contributed equally.

https://doi.org/10.1016/j.biomaterials.2021.121187
Received 19 July 2021; Received in revised form 8 October 2021; Accepted 14 October 2021
Available online 18 October 2021

cellular fractions or a combination thereof [3].

Assessing new potential therapies for bone defect repair begins with *in vitro* systems or *ex vivo* systems, since they are inexpensive and relatively simple [4]. However, they are limited since their simplicity comes with the price of excluding major cellular types involved in the process of bone regeneration. Thus, in order to further study the dynamics of bone formation and regeneration, the next step requires the use of preclinical animal models. These *in vivo* models are classified according to the site where bone formation takes place, at either orthotopic or ectopic locations [5]. In rodents, orthotopic locations such as at the radius, calvarium and the femur are nowadays the gold-standard for orthopaedic research as they are the most clinically relevant, in that they involve the creation and healing of a defect in a bony environment [6]. These studies are however time consuming, expensive, have a large impact on animal welfare due to the invasive nature of the model and require advanced surgical procedures. As an alternative, is it long known that *de novo* bone formation can be induced and studied at ectopic locations if three elements are provided: an inducing agent, an osteogenic precursor cell and an environment which is permissive to osteogenesis [7]. Common methods used for this purpose are based on intramuscular and subcutaneous implants, the latter being the easiest to perform surgically and having the lowest impact on animal welfare. Unlike orthotopic locations though, ectopic bone formation is not initiated by an established bony microenvironment, which poorly models some aspects of bone defect repair and an evaluation of the integrative repair capacity of the graft with the adjacent tissue is not possible.

Due to the increasing numbers of novel bone grafts being developed in the last years and the ethical concerns that animal experimentation raises, it is desirable to develop new experimental models aiming for surgical simplicity that improve the animal welfare and allow the simultaneous testing of multiple grafts in a controlled environment. To address this, we hypothesised that a piece of bovine bone subcutaneously implanted in an immunodeficient mouse would retain the ability to regenerate -by recapitulating the events of bone repair- and thus, that it could be potentially used as a bone graft screening tool. For this reason, in this work we aimed to develop a new minimally invasive "semi-orthotopic" bone defect model for cell and biomaterial testing in regenerative medicine that would combine the advantages of ectopic and orthotopic bone repair models.

2. Materials and methods

2.1. Preparation of the bone ring constructs

Bone rings were prepared from freshly harvested distal epiphyses of the metacarpal bones of 3 to 8-month-old calves, which were purchased from a slaughterhouse and processed within 5 h. To produce the rings, the metacarpophalangeal joint (MCP) was opened, and the cruciate ligaments sectioned, to expose the articular cartilage surfaces. Next, 10 hollow cylindrical osteochondral plugs per bone were drilled by using an 8 mm diameter trephine drill [MF Dental, Weiherhammer, Germany] in which a central canal was drilled using a 3-, 4- or 5-mm steel drills. Tissue damage was minimised by avoiding the heating of the explant though low speed drilling and simultaneous cooling with sterile PBS. Then, 4 mm height rings were made by removing the articular cartilage and the proximal bone ends using a circular table saw. In this way, 8-mm diameter x 4-mm height bone rings were obtained. Next, the bone rings were transferred to 12-well plates containing α-MEM supplemented with 10% v/v FBS, 100 μg/mL gentamycin and 3 μg/mL amphotericin B [all from Thermo Fischer, Bleiswijk, The Netherlands] and incubated overnight in a humidified atmosphere at 37 °C and 5% CO_2. The following day, immediately before implantation, the cores of the rings were filled with the different grafts. The top and bottom ends of the rings were closed with two circular 8 mm diameter dense polytetrafluoroethylene membranes (dPTFE) [PermaMEM®, Botiss biomaterials, Zossen, Germany], to prevent direct in-growth of host cells into the testing pocket and fastened with a single 6–0 non-resorbable polyamide suture Ethilon® [Johnson & Johnson Medical, Livingston, UK]. (Fig. 1A and B). The viability of the explants at the moment of implantation was assumed, since previously observed that comparable explants obtained in a similar manner remain viable *in vitro* for one month [8].

2.2. Preparation of the different grafts

To validate the model, different grafts were prepared to modulate bone formation inside the defect: cortical bone chips, tissue engineered cartilage constructs and cartilage grafts.

2.2.1. Cortical bone chips

The leftover bones used to produce the bone rings were used to harvest bone chips. After removal of the periosteum, the cortical surface of the diaphysis was scraped with a Safescraper® Twist [Geistlich Sons Lt., Manchester, UK] [9], and the scraped chips were placed in α-MEM supplemented with heat inactivated 10% v/v FBS, 100 μg/mL gentamycin and 3 μg/mL amphotericin B [all from Thermo Fischer, Bleiswijk, The Netherlands], and incubated overnight in a humidified atmosphere at 37 °C and 5% CO_2.

2.2.2. Tissue engineered cartilage constructs

Bone marrow stromal cells (MSCs) were isolated from leftover iliac crest bone chip material obtained from a 9-year-old male paediatric patient undergoing alveolar bone graft surgery (with institutional consent for the use of waste surgical material with the option for parental opt-out and approval of medical ethics committee of Erasmus University Medical Center: MEC-2014-16). Cells were expanded in αMEM containing heat inactivated 10% v/v FBS and supplemented with 50 μg/mL gentamycin, 1.5 μg/mL amphotericin B, 25 μg/mL L-ascorbic acid 2-phosphate [Sigma, Zwijndrecht, the Netherlands] and 1 ng/mL fibroblast growth factor-2 [Bio-Rad via Bioconnect, Huissen, the Netherlands] in a humidified atmosphere at 37 °C and 5% CO_2. The ability of these cells to differentiate into multiple tissues was confirmed by trilineage differentiation (data not shown), as described previously [10].

2.2.2.1. Generation of chondrogenic pellets. To generate the chondrogenic pellets, 2 x 10^5 MSCs (passage 3) were suspended in 500 μL of chondrogenic medium (high-glucose Dulbecco's modified Eagle's medium (DMEM) [Thermo Fischer, Bleiswijk, The Netherlands] supplemented with 50 μg/mL gentamycin, 1.5 μg/mL fungizone, 1 mM sodium pyruvate [Thermo Fischer, Bleiswijk, The Netherlands], 40 μg/mL L-proline [Sigma, Zwijndrecht, the Netherlands], 1:100 v/v insulin-transferrin-selenium [ITS+; BD Biosciences], 10 ng/mL transforming growth factor β3 [R&D systems], 25 μg/mL L-ascorbic acid 2-phosphate, and 100 nM dexamethasone [Sigma, Zwijndrecht, the Netherlands]) in 15 mL polypropylene tubes [TPP via Westburg], and centrifuged at 300 g for 8 min. The pellets were chondrogenically differentiated for 23 days, where the chondrogenic media was replaced twice weekly.

2.2.2.2. Cell seeded scaffolds. To fabricate highly porous collagen-based scaffolds, a lyophilisation method previously described by O'Brien FJ et al. was used [11]. Type I collagen-GAG scaffolds were composed of type I collagen derived from bovine Achilles tendon [Collagen Matrix, USA] and chondroitin 6-sulfate (CS) derived from shark cartilage [C4384, Sigma-Aldrich, Ireland]. Briefly, collagen-GAG slurry was prepared by dissolving 3.6 g collagen and 0.32 g of CS in 360 ml of 0.5 M acetic acid using a blender [Ultra Turrax T18 Overhead Blended, IKA Works Inc., USA] at 15,000 rpm for 90 min at 4 °C. The final concentrations of the suspension were composed of 0.5% (w/v) collagen and 0.05% (w/v) CS. Subsequently, 0.3 ml of the slurry was pipetted into a stainless-steel tray (internal dimensions: 9.5 mm diameter and 4 mm height) before being freeze-dried [Virtis Genesis 25 EL, Biopharma, UK]

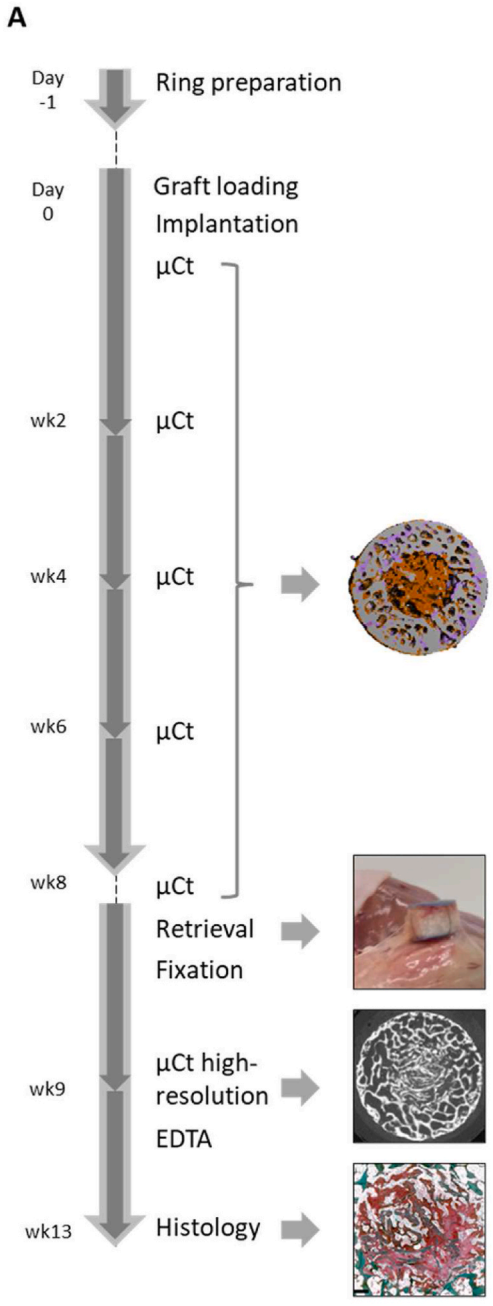

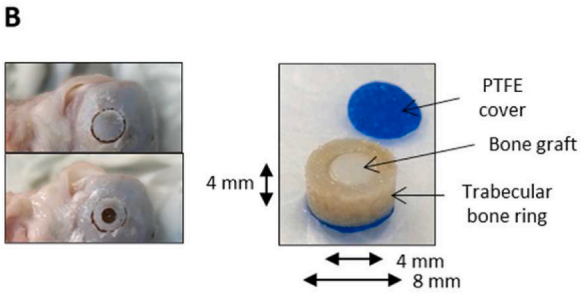

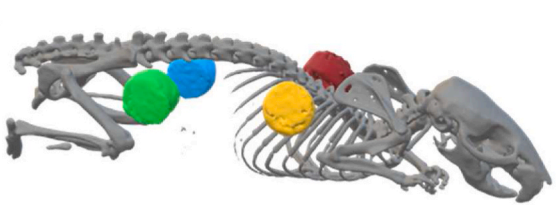

D

Test aim	Filling	Purpose
Model validation (ossification)	Empty	Neg. Control
	Bone chips	Pos. Control
Bone tissue engineering stratey	MSC pellets	Cellular approach (endochondral)
	Collagen scaffold	Biomaterial approach
	Collagen scaffold with MSCs	Combined cell-biomaterial approach
Graft permisiveness to ossification	Hyaline cartilage	Neg. Control
	Processed hyaline cartilage	Pos. Control

Fig. 1. *Preparation of the semi-orthotopic bone defect model.* (A) Experimental timeline (B) Ring preparation and parts of the construct (C) Full-body micro-CT of a mouse hosting four constructs, highlighted in different colours (D) Construct fillings and purposes (E). Micro-CT (µCT); Negative (Neg.); Positive (Pos.). (For interpretation of the references to colour in this figure legend, the reader is referred to the Web version of this article.)

at a constant cooling rate of 1 °C/min to a final temperature of −40 °C. Next, the porous scaffolds were dehydrothermally crosslinked in a vacuum oven [VacuCell, MMM, Germany] for 24h at a pressure of 0.05 bar and temperature 105 °C. In order to prepare the scaffolds to be seeded with cells, the scaffolds were rehydrated with graded ethanol series (100%, 90%,70%) to dissolve acid residues. Then, they were washed with distilled water and PBS prior to cell seeding. The scaffolds, measuring dry 1 cm × 1.5 cm x 3 mm, were seeded each with a 0.5 ml suspension of $2x10^6$ MSCs (passage 3) while contained inside 50 ml polypropylene tubes. 30 min later, 4 ml chondrogenic medium was added to the tubes. Next day, the scaffolds were transferred to polystyrene suspension culture plates [Greiner Bio-One] in chondrogenic medium. Media was refreshed twice weekly during the 23-day culture period. If cellular outgrowth was observed from the scaffold, the scaffolds were transferred to a new suspension plate. Since the cellular activity within the scaffolds during the culture time caused the scaffolds to contract reducing their volume, two cell-seeded scaffolds were implanted per bone ring to completely fill the defect.

2.2.2.3. Cartilage grafts. Tracheal explants were obtained from 3 to 8-month-old calves, purchased from a slaughterhouse. To prepare them, adjacent tracheal rings were dissected and sectioned sagitally at 4-mm intervals; then, transverse cylindrical biopsies were obtained with a 4-mm diameter biopsy punch [Stiefel Laboratories, Durham, NC] to obtain cartilaginous pieces that fit tightly into the whole volume of the bone defect. Viable cartilage samples were kept overnight until implantation in high-glucose DMEM supplemented with 100 µg/mL

gentamycin and 3 μg/mL amphotericin B. In parallel, a set of explants were devitalised by performing 5 freeze-thaw cycles at −21 °C, 60 min each and extracted for 16 h in 4 M guanidine hydrochloride (GuHCl) [Sigma-Aldrich] under agitation at room temperature. Last, residual GuHCl was removed by three washes in PBS followed by a 4h incubation in PBS. One cylinder was implanted per bone ring.

2.3. Surgical implantation procedure and longitudinal micro-CT imaging

Animal experiments were conducted in the experimental animal facility of the Erasmus University Medical Center with approval of the local animal ethics committee (under licence number 101002015114 and protocol number 15-114-09), which comply with EU Directive 2010/63/EU, and were reported in compliance with the ARRIVE guidelines. The surgical procedure was performed on 10- to 14-week-old male immunodeficient NMRI-Foxn1 nu/nu mice purchased from Janvier [Le Genest-Saint-Isle, France]. This strain has previously been shown to be capable of hosting similar xenogeneic implants [12–14]. 16 mice were used in total. This included experimental conditions from another study whereby the same control conditions were used in order to reduce total animal numbers. Of the 64 available subcutaneous pockets in these 16 mice, 40 pockets were used specifically for the study reported here. Mice were housed in groups of 3 and 4 in individually ventilated cages, and food was provided *ad libitum*. To avoid peri- and post-operative pain, mice received 0.05 mg/kg body weight of buprenorphine [Reckitt Benckiser, Hull, UK] 1 h before the operation and 6–8 h after implantation. The operation was performed under isofluorane inhalation anaesthesia. During the procedure, four incisions were made on the back of each mouse to create four subcutaneous pockets, where four constructs per mouse were placed bilaterally with respect to the thoracic and lumbar vertebrae. To prevent confounding effects, all experimental replicates and corresponding conditions for direct comparison were implanted in the same batch of surgeries and each treatment replicate was placed in each of the four pocket positions, ensuring that no more than two treatment replicates were placed in the same mouse. No blinding was performed. After construct placement, 4–0 non-resorbable polyamide suture Ethilon® [Norderstedt, Germany] was used to close the wounds. While still under anaesthesia, the four implants were scanned by micro-CT [Quantum GX, PerkinElmer, USA], with a 36 mm Field of View (FOV) and 72 μm isotropic voxel size. After the scan, the sutures were immediately replaced by clips [AutoClips®, Fine Science Tools, Heidelberg, Germany], since the clips would otherwise introduce artifacts into the scan, and the mice received an injection of 25 mg/kg of ampicillin [Dopharma, Raamsdonksveer, The Netherlands]. The clips were removed 8–10 days after the operation, when the wounds had healed. At 2, 4, and 6 weeks after the surgical procedure, mice were scanned again under isofluorane anaesthesia. After 8 weeks, mice were sacrificed by cervical dislocation under isofluorane anaesthesia, scanned again and the constructs retrieved. The bone rings were fixed in 4% buffered formalin at room temperature for one week. During fixation, the caps were removed and the constructs were scanned again by the micro-CT for 4 min with a FOV of 18 mm and 36 μm isotropic voxel size. During the entirety of the experiment, the health condition of the mice used was closely monitored, and a humane endpoint was established if there was a drop in body weight of 15% in 2 days or 20% from the moment immediately after implantation. Moreover, the exclusion of all constructs from analysis was set up *a priori* if the humane endpoint was reached. No signs of distress were evident, all the mice survived and all the conditions intended for this study were included for analysis.

2.4. Micro-CT analysis

2.4.1. Bone volume of the whole constructs

Bone morphometric analysis of the DICOM images generated was performed using specialized micro-CT software [SCANCO Medical AG, Brüttisellen, Switzerland]. Phantoms of known densities (0.25 g/cm^3 and 0.75 g/cm^3) were scanned at every measurement and used to convert pixel intensity into mineral density. To assess the total bone volume of each construct, the bone region was segmented from the neighbouring tissues using an automated contouring method. The resulting grey-scale images were Gaussian filtered with sigma of 0.8 and a support of 1 voxel, and the signal above a density threshold of 335 mg HA/ccm was used to produce binary images (Suppl. Fig. 1). Then, the bone morphometric parameter bone volume (BV) was evaluated using a three-dimensional analysis software [Image Processing Language, SCANCO Medical AG, Brüttisellen, Switzerland].

2.4.2. Automatic co-registration of follow-up scans and longitudinal bone morphometric analysis of the construct's testing pocket

Changes over time in the bone microarchitecture were determined by overlaying two consecutive data sets, provided that these have equal orientations. As the trabecular microarchitecture of the bone rings experienced only minor changes during the experiment, their 3D volumes were used to perform landmark-free alignments on the series of longitudinal scans (Suppl. Fig. 2). For this, the segmented binary images previously obtained were first used to create 3D reconstructions. Then, each follow-up scan was aligned to its corresponding initial scan by automatic rotation and translation based on iterative transformations, so the overlapping volume was maximised between the two. This analysis was based on a previously described method [15,16]. Following alignment, clusters of voxels were compared and categorised as either bone gain (only present in the follow up image), bone loss (only present in the baseline image) or unaltered bone volume (present in both images). Afterwards, color-coded images were created to represent those three categories. Next, in order to analyse the bone morphometric parameters of the testing pocket, the inner defect volume of the baseline scan was automatically segmented using a self-generated algorithm. Then, each of its follow-up scans was automatically aligned, and the baseline segmentation transferred to them. After calibration with hydroxyapatite (HA) phantoms of known density, the signal above a density threshold of 335 mg HA/ccm was used to produce binary images (Suppl. Fig. 1). The BV was calculated, and in order to compensate for minor differences in the manufacturing between the different rings, the ratio between the BV and the total volume of the defect (TV), the BV/TV, was calculated.

2.5. Histological assessment

After fixation, the constructs were decalcified in 10% w/v ethylenediaminetetraacetic acid (EDTA) pH 6.8–7.2 at room temperature for 4–5 weeks, where the EDTA was refreshed twice weekly. Subsequently, the samples were embedded in paraffin and 6 μm thick sections were collected for histology at different depths. Before histological assessment, sections were deparaffinised using a series of xylene, graded ethanol (100%, 96% and 70%) and distilled water.

2.5.1. H&E staining

The histological sections were stained with Gill's haematoxylin [Sigma-Aldrich] for 5 min and incubated in 2% w/v eosin [Merck, Amsterdam, The Netherlands] in 50% v/v ethanol and 0.5% v/v acetic acid for 45 s. The sections were incubated in 70% ethanol for 10 s and afterwards dehydrated in 96% ethanol for 1 min, 100% ethanol for 1 min and two times xylene for 1 min, after which they were mounted with DPX, coverslipped and dried overnight at 37 °C before imaging.

2.5.2. RGB staining

RGB trichrome staining was performed as described by Gaytan F et al. [17]. Briefly, sections were dewaxed using xylene and graded ethanol, rinsed in distilled water and stained for 20 min in 1% w/v Alcian Blue 8GX [Sigma] in 3% v/v acetic acid at pH 2.5. Then rinsed in tap water, followed by 20 min 1% w/v Fast Green [Sigma] in distilled water. Then, they were rinsed for 5 min in tap water, followed by 30 min 1% w/v Sirius Red [Direct Red 80, Sigma] in a saturated aqueous

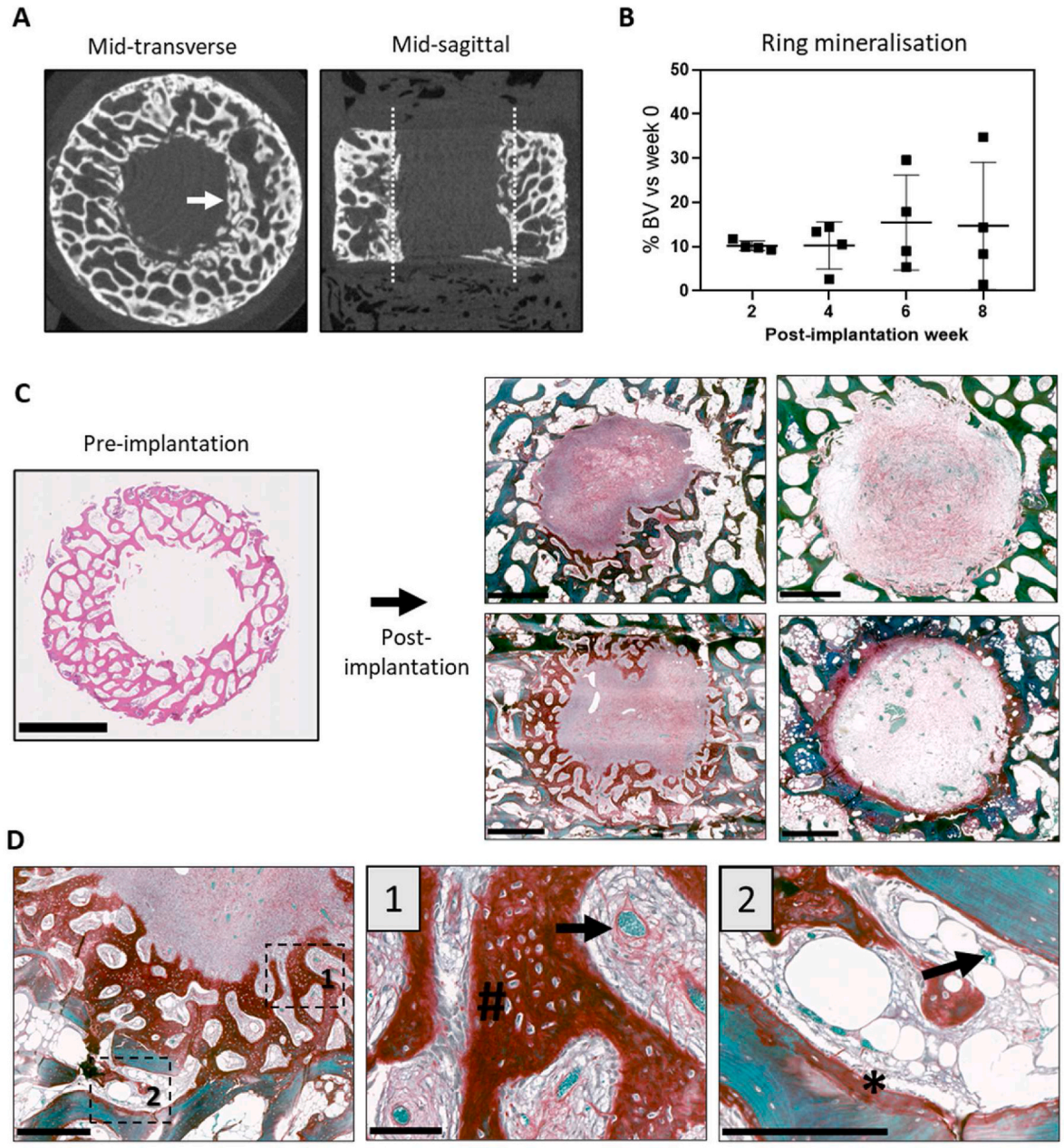

Fig. 2. *Bone formation into an empty defect in the semi-orthotopic bone ring healing model after 8 weeks in vivo*. (A) Micro-CT showing the mid-transverse and mid-sagittal planes of one construct 8 weeks post-implantation. White arrow and dotted lines indicate a region with newly formed bone. (B) Percentage of the whole cylinder's bone volume (%BV) over time versus the bone volume at the time of implantation. N = 4 constructs per condition. (C) H&E staining showing the rings pre-implantation and RGB staining showing different degrees of closure in representative sections of 4 different constructs 8 weeks post-implantation. Scale bars: 1 mm. (D) RGB staining showing bone formation takin place both inside the defect (1) and on the pre-existing bone of the ring (2). The hash (#) indicates calcified cartilage undergoing endochondral bone formation. In green the mature bone; the asterisk (*) marks the osteoid and the black arrows mark the presence of blood vessels in light green. Scale bars: E: 500 μm, E_1: 250 μm, E_2: 100 μm. (For interpretation of the references to colour in this figure legend, the reader is referred to the Web version of this article.)

solution of picric acid. Then sections were carefully rinsed twice in 1% v/v acetic acid (3min each wash), followed by dehydration in subsequently 100% Ethanol (2x) and two times in Xylene. Slides were covered with DPX, coverslipped and dried overnight at 37 °C before imaging.

2.5.3. Tartrate resistant acid phosphatase (TRAP) staining

Sections were incubated for 20 min at room temperature in freshly prepared 0.2 M acetate buffer, 100 mM L (+) tartaric acid pH 5.0. Then to this acetate buffer 0.5 mg/ml naphthol AS-BI phosphate [Sigma] and 6.4 mg/ml Fast Red TR salt [Sigma, 15% dye content] was added. Sections were incubated for 1–1.5 h at 37 °C and regularly checked until cells stained bright red. After staining sections were rinsed with distilled water and lightly counterstained with Haematoxylin (Gill's formula), followed by a 10 min wash with running tap water and dried overnight at 37 °C. Sections were coverslipped with VectaMount® and imaged.

2.5.4. Safranin O staining

Sections were incubated in 0.1% Light Green solution [Sigma-Aldrich] in distilled water for 8 min. Afterwards they were rinsed with 1% acetic acid. Then, the slides were incubated with 0.1% Safranin O solution [Fluka] in distilled water for 12 min. They were rinsed two times with 96% ethanol for 30 s and afterwards dehydrated in 100%

ethanol for 1 min and two times xylene for 1 min. Sections were coverslipped with VectaMount® and imaged.

2.6. Image acquisition

Composite tile scans from stainings were obtained with a NanoZoomer HT microscope (C9600-12) using the software NDP.scan v2.5.90 [Hamamatsu Photonics]. Hue and brightness were adjusted after acquisition using Adobe Photoshop CC 2018, following the recommendations described by Sedgewick [18].

2.7. Statistical analysis

Each construct was treated as a separate unit for means of measurement, independently of the position and the identity of the host mouse. Mice were considered as carriers of the constructs, and their interindividual variability assumed to play a negligible role into the construct's response to the graft. Normality of the data was not assumed for the analysis of longitudinal micro-CT measurements. Longitudinal measurements versus the initial timepoint within same sample were analysed by Kruskal-Wallis test with Dunn's correction. Single terminal time point data was compared via Mann-Whitney two-tailed test.

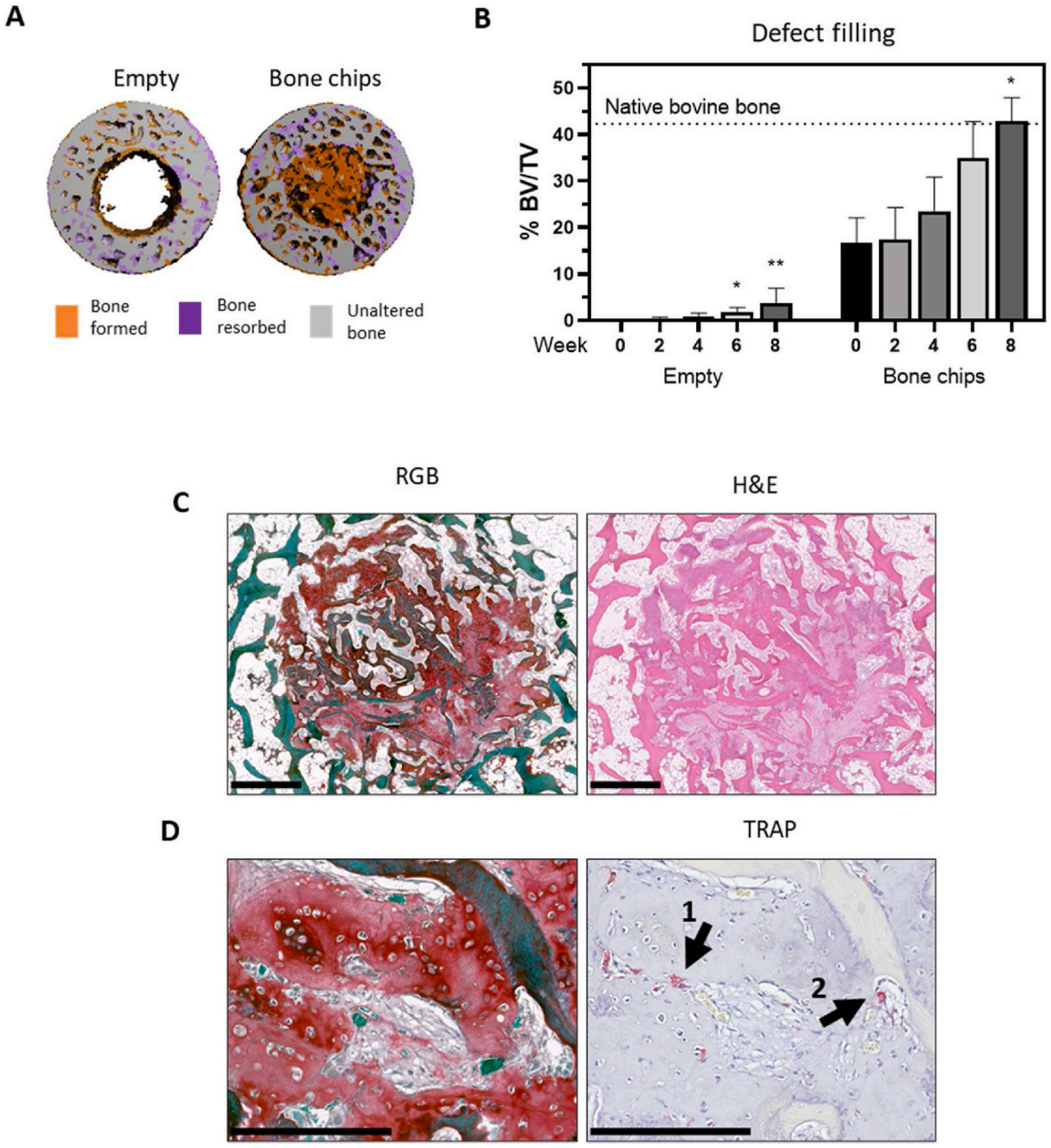

Fig. 3. *Assessment of the healing capacity of the construct in the semi-orthotopic bone defect healing model.* (A) Pre- and post-implantation overlays of micro-CT 3D image reconstructions. (B) Quantification of mineralization over time per volume unit (% BV/TV) inside the defect when empty and when cortical bone chips are used as grafting material. Dotted line indicates the average undamaged bovine bone pre-implantation % BV/TV. The two conditions were analysed separately, and time points were compared by one-way ANOVA. N = 4 constructs per condition. Bars indicate average +SD. *$p < 0.05$, *$p < 0.01$ (vs. week 0). (C) Serial sections with RGB and H&E stainings showing the presence of mature bone and forming bone inside the defect post-implantation via endochondral ossification. Scale bar 1 mm. (D) Serial sections with RGB and TRAP stainings. Arrows point at TRAP + cells remodelling the newly-formed matrix (1) and the cortical bone used for grafting (2). Scale bar 250 μm.

Longitudinal measurements where the change in the bone filling of the defect in time of two conditions was compared, were analysed by paired analysis by two-way ANOVA with time matching. Sphericity was assumed and Sidak correction for multiple comparisons was performed. A p-value of <0.05 was considered significant. GraphPad Prism (version 8.0.1 for Windows, GraphPad Software, La Jolla California USA) was used to perform the statistics and to create the graphs.

3. Results

3.1. Bone rings can recapitulate critical size defects in vivo

In order to determine what defect size could be considered as critical in our model, we assessed the spontaneous ossification taking place in constructs containing different defect sizes over a period of 8 weeks. For this, we implanted different constructs incorporating empty defects of 3 mm, 4 mm and 5 mm following the methodology described in Fig. 1. No noticeable adverse effects occurred on these mice, nor the rest used for this study. Following implant placement and until termination of the experiment, all the mice of the study increased their weight by 7.6% ± 5% (Suppl. Fig. 3). After 8 weeks, the micro-CT images and histological inspection revealed that *de novo* bone formation had taken place inside the defects, although the bone deposition was limited to the inner edges of the ring (Suppl. Fig. 4). Since the 3 mm defect was mostly occluded by the new bone formed, and to maximise the amount of marrow to better replicate the bone microenvironment, the 4 mm defect was selected to be used in further experiments. Next, we assessed in more detail the biological processes taking place *in vivo* in those constructs. After 8 weeks, mineralised projections of the ring into the defect could be observed by micro-CT at different depths, indicating that new calcified tissue was being formed inside the defect adjacent to the inner ring surface (Fig. 2A). In addition, the total mineral content of the implanted ring increased on average around 15% during the 8-week period of implantation (Fig. 2B). The histological analysis after comparison to the construct pre-implantation (Fig. 2C) revealed that vascularised fibrous tissue had formed inside the ring during implantation, initiating the closure of the defect (Fig. 2C). A closer look at the defect site revealed that the bony projections observed with the micro-CT images corresponded to newly formed mineralised matrix. The histology suggested that bone was forming via endochondral ossification (Fig. 2D). The newly formed bone was well-integrated to the bone ring and had formed vascularised marrow compartments. In addition, more bone had formed inside the trabecular space of the ring too (Fig. 2D), which also contributed to the increase of the total calcified volume of the construct. In conclusion, these observations indicated that the bone rings retained their inherent ability to regenerate, but to a level insufficient to heal the full defect during the 8-week timeframe. Consequently, this opened the possibility that bone formation could be stimulated if a suitable bone graft was placed into the defect.

3.1.1. Bone formation is stimulated when a suitable graft is placed into the defect

In clinics, autologous bone chips are the gold standard used for bone augmentation due to their osteoconductive, osteoinductive, and osteogenic properties. For this reason, we next validated the model by testing if a graft composed of bovine cortical bone chips would have the ability to increase the rate of bone formation inside the ring's defect more than if left empty. The micro-CT overlay of the constructs before and after implantation indicated that most of the newly calcified tissue in the condition containing the bone chips localised inside the defect (Fig. 3A). This result suggested the ability of the defect to regenerate when a suitable graft was placed inside. In order to assess the net gain in bone volume experienced over time, the amount of calcified tissue present in the defect was quantified by applying the analysis algorithm described in Suppl. Fig. 2. After 8 weeks, while the empty defects filled their mineralised bone volume by 4 ± 3%, the defects that were implanted with bone chips (corresponding to an initial 17 ± 5% filling) experienced a net bone volume increase of 26 ± 8%, reaching in total the same average level of bone volume per volume unit as the native bovine bone used to manufacture the rings, 42% mm^3/mm^3 (Fig. 3B). This was further confirmed by histology (Fig. 3C), where large amounts of forming bone via endochondral ossification (in red) and mature bone (in green) were present inside the defect and surrounded by a newly formed marrow containing blood vessels, adipocytes and other cell types. Among those, multinucleated bone lining TRAP + cells, indicative of osteoclasts, were observed remodelling both the newly formed matrix and the cortical bone used for grafting. In order to ensure that the signal measured on micro-CT corresponded to that of the histological observations, the resulting signals at matching locations were compared (Suppl. Fig. 5). From all the above, we concluded that it is possible to evaluate the healing dynamics of the bone ring defect when a suitable graft is placed inside.

3.1.1.1. Bone formation occurs in tissue engineered constructs. Cell based tissue engineering approaches, particularly focused on the developmental process of endochondral ossification are a very commonly used method for bone defect repair. Next, we further tested the feasibility of the model by investigating cell-based and cell-free approaches for bone defect repair. We first evaluated if small spheres of hypertrophic cartilage grafts derived from bone marrow stem/stromal cells (MSCs) could undergo endochondral ossification. To produce such grafts, MSCs were chondrogenically differentiated in the pellet system [10,19]. The histological analysis confirmed that chondrogenic differentiation had taken place, by the blue coloration of the RGB staining (Fig. 4a), by the cellular hypertrophy and by Safranin O staining (not shown). Then, 9 to 11 of those spherical pellets were placed inside each bone defect to fill the maximum volume possible. After 8 weeks *in vivo*, it was possible to observe with micro-CT that the cartilaginous constructs had induced mineralised tissue formation inside the defects (Fig. 4B and C). Histological assessment revealed that bone formation was taking place both between and within the pellets (Fig. 4D). Since different rates of ossification took place between constructs, the differences in colour unveiled that the spaces between pellets ossified at a faster pace than the pellets themselves. In addition, TRAP + cells could be identified remodelling the cartilage matrix of the MSC constructs (Fig. 4E). In a second group, highly porous scaffolds prepared with collagen type I in combination with chondroitin sulfate, which have previously shown potential for bone regeneration when implanted [20–22]. Scaffolds were seeded with MSCs and cells chondrogenically differentiated *in vitro*. After confirmation of the deposition of a cartilaginous matrix (Fig. 4F), the constructs were implanted for 8 weeks *in vivo* in parallel to the same cell-free scaffold, in order to compare a cell-free and a cell-seeded scaffold. The CT analysis at 8 weeks revealed that both, the cell-free and cell-seeded scaffolds had calcified and performed similarly with regard to bone formation (Fig. 4G and H). This was further verified by histology, suggesting that bone was forming via endochondral ossification in both conditions (Fig. 4I). These experiments supported that the osteogenic performance of grafts composed of solely biomaterial, solely cells, or a combination of biomaterials and cells can be studied effectively in our model.

3.1.2. Graft permissiveness to ossification

Since the bone ring demonstrated the ability to possess intrinsic osteoinductive properties, we then explored if our model could be used to assess graft's permissiveness to osteogenesis and vascularisation. For this, tracheal cartilage was used. Contrary to the transient cartilage constructs produced with MSCs, young tracheal cartilage remains phenotypically stable by actively preventing blood vessel invasion and subsequent ossification [23]. In order to produce comparable tracheal grafts that permit ossification, we hypothesised that devitalising and extracting a subset of these tracheal grafts would result in the loss of

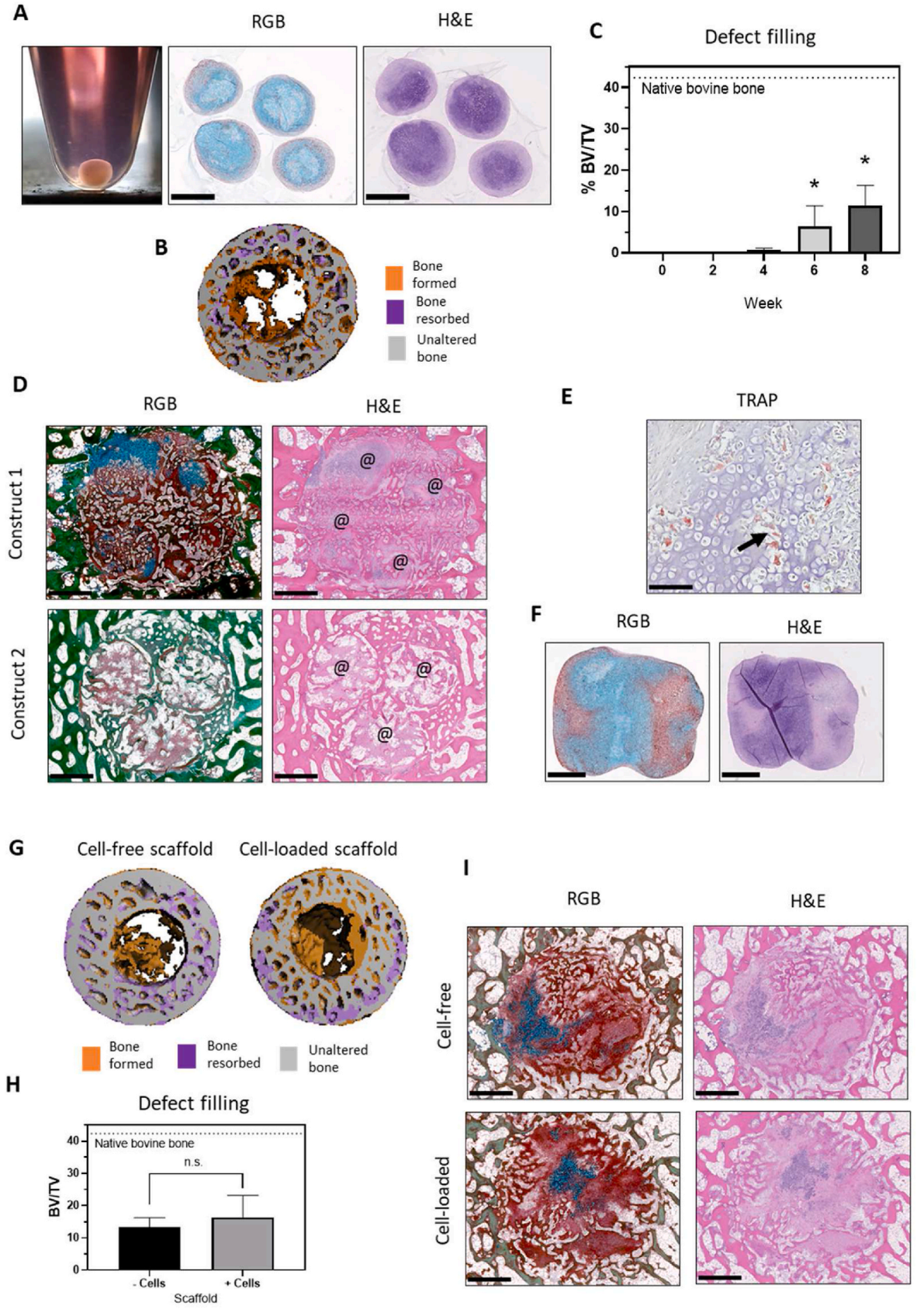

(caption on next page)

Fig. 4. *Different tissue engineering approaches grafted in the semi-orthotopic bone defect healing model.* (A) Macroscopic view and RGB and H&E stained chondrogenically primed (for 23 days) MSC pellets prior to implantation. (B) Pre- and post-implantation overlays of micro-CT 3D image reconstructions. (C) Quantification of mineralization measured by micro-CT over time per volume unit (% BV/TV) inside the defect when pellets were used as grafting material. (D) RGB and H&E-stained sections showing two different constructs post-implantation that are at different stages of ossification. @ Indicates the location of the pellets. (E) TRAP staining demonstrating active remodelling of the pellets inside the defect. Arrow indicates a group of TRAP + cells resorbing the matrix (F) RGB and H&E-stained cell-seeded scaffolds chondrogenically primed for 23 days prior to implantation (G) Pre- and post-implantation overlays of micro-CT 3D image reconstructions of cell-free and cell-loaded scaffolds (H) Quantification of mineralization per volume unit (% BV/TV) inside the defect 8 weeks post-implantation (I) RGB and H&E-stained scaffolds showing the healing defects post-implantation. Scale bars, A, D, F, I: 1 mm, E: 100 μm. Bars indicate the SD. In C, N = 4; in H, N = 6. *p < 0.05 (vs. week 0); n.s. (non-significant) p < 0.05.

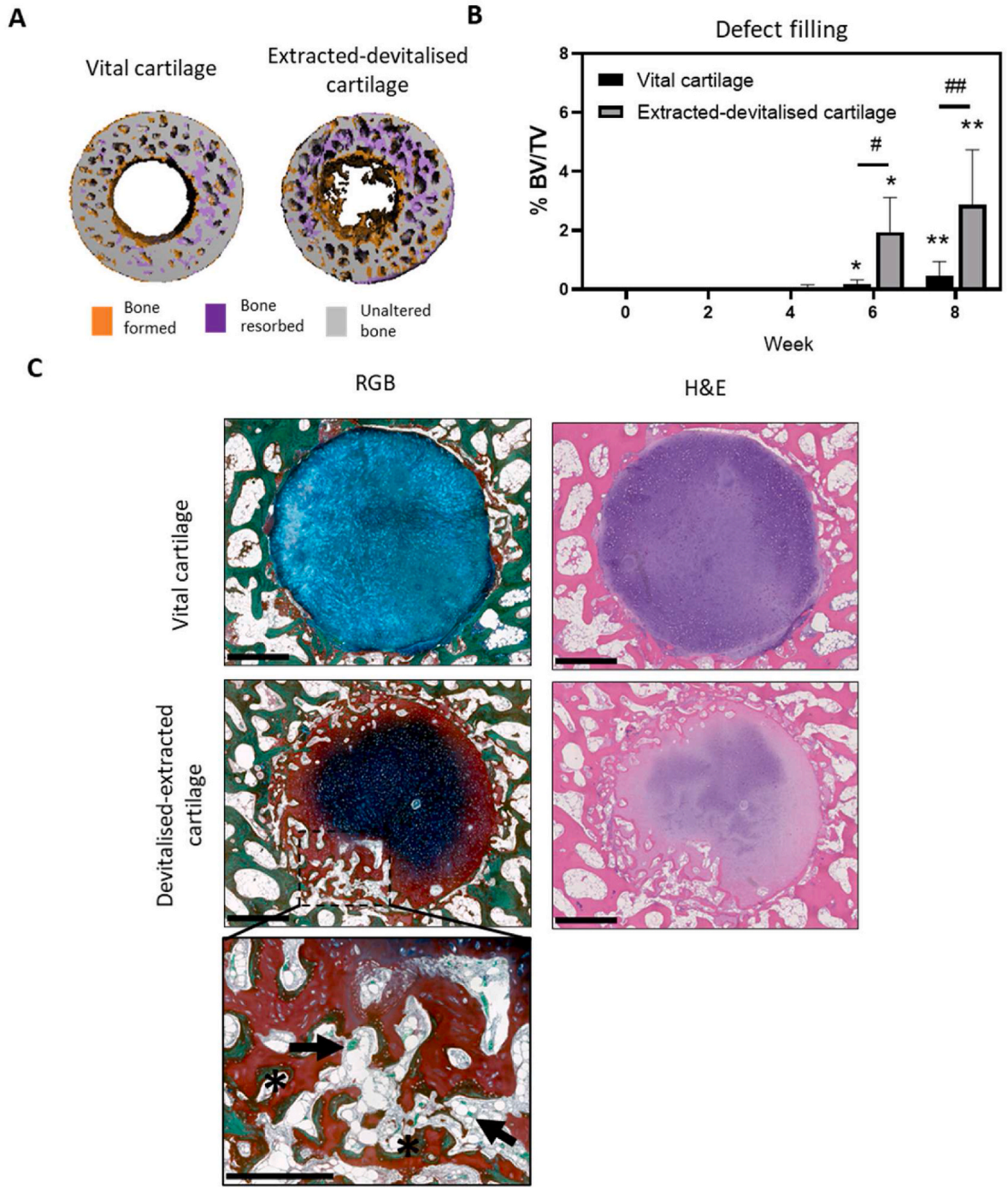

Fig. 5. *Evaluation of graft permissiveness to ossification in the semi-orthotopic bone defect healing model.* A) Pre- and post-implantation overlays of micro-CT 3D image reconstructions. B) Quantification of bone volume over trabecular volume in the defect area filed with vital or extracted cartilage. N = 4 constructs per condition. Bars indicate the SD. *p < 0.05, *p < 0.01 (vs. week 0); #p < 0.05, ##p < 0.01 (matched timepoints). C) RGB and H&E stainings after 8 weeks of the vital or extracted cartilage. The asterisk (*) marks the newly deposited bone and the black arrow marks the presence of a blood vessel in light green. Scale bars, 1 mm and 500 μm. E: 100 μm. (For interpretation of the references to colour in this figure legend, the reader is referred to the Web version of this article.)

their anti-invasive properties. Then, the rings were loaded with both vital and devitalised-extracted tracheal cartilage grafts. Eight weeks post-implantation, the devitalised-extracted cartilage showed a significant increase of mineralization on micro-CT in comparison to the vital cartilage, suggesting that the devitalised-extracted cartilage was undergoing remodelling (Fig. 5A and B). Histological analysis revealed that the vital cartilage grafts had remained phenotypically stable, as demonstrated by the strong GAG staining, the absence of blood vessels and bone projections (Fig. 5C). In contrast, the devitalised-extracted grafts displayed extensive remodelling originated from the bone ring (Fig. 5C). Large number of erythrocytes were visible in the devitalised-extracted cartilage graft, indicating it had spontaneously vascularised. In addition, new marrow compartments and mineralised structures had occurred. These observations demonstrated that this model can be used to assess the permissiveness of grafts to vascularise and undergo osteogenic remodelling.

4. Discussion

In this work we have developed a new *in vivo* semi-orthotopic bone defect healing model for the purpose to test cell, bioactive molecules, biomaterials –and combinations thereof– for regenerative medicine. By ectopically implanting bovine bones containing a critical-size defect in a mouse, we have demonstrated the potential for at least four standardised osteoinductive microenvironment in a single animal. This will allow the evaluation and comparison of desirable biological processes that take place during graft-mediated bone healing, opening the possibility to be used as a new *in vivo* medium throughput screening platform. Since this platform offers great reproducibility, can be automated and thus, lower costs, it is expected to allow a more efficient testing of bone grafts in rodents, with special emphasis on the principles of the 3Rs (reduction, replacement and refinement) [24].

Traditionally, fracture healing has been studied in large animals such as dogs, rabbits and sheep due to their large skeletal size and similar bone structure to humans. Due to the excessive costs, research started to move first to rats and then further to mice [25], since these animals offered technical advantages such as easy handling, reduced prices and a large *repertoire* of genetically modified strains. Nevertheless, the reduced size of the mouse limits the volume of the graft that can be tested. Our semi-orthotopic *in vivo* model suggests however that it is possible to overcome some of the current limitations that mice pose. In particular, regarding the number and size of bone grafts that can be tested simultaneously at orthotopic locations, and allowing the evaluation of 4 grafts per mouse, each containing a 50 mm^3 bone defect. By contrast, previous mouse critical-size defect models were reported as single 3 mm length defects (<3 mm^3) [26], while double calvarial defects were produced by drilling two 3.5 mm diameter defects (<3.4 mm^3, as calculated from the values provided in Ref. [27]). By comparison, our model is closer to the orthotopic bone defect sizes used in rabbits (70–100 mm^3) [28–31]. With our new model, we have the added beneficial capability of not only testing bigger constructs in mice –allowing to replace larger animals for smaller ones in specific set-ups– but also having controls within the same animals as a treatment condition, thus reducing inter-animal variability and potentially the number of animals required. Moreover, the ectopic location of the four testing units constitutes a refinement of the current orthotopic surgeries, since the implanted constructs lack functional pain receptors and the animal locomotion remains unaffected. An additional advantage of our model is the possibility to generate micro-CT scans *in vivo*. As the same animal can be imaged at different time points, this limits the number of animals needed and enables the use of image registration to increase the sensitivity of the results. It should be noted that in this study a relatively low threshold was used (335 mgHA/ccm) that not only segments bone but also low-mineralised tissue. Using this low threshold makes the model more sensitive for the detection of mineralization in the defect region, but also results in an overestimation of trabecular thickness and the bone volume fraction in the ring of original bone. It would be possible, however, to use a dual-threshold to differentiate between low-mineralised and fully mineralised bone.

The capacity of a human bone construct to initiate its regenerative program *in ovo* was demonstrated by Moreno-Jimenez et al. [32], in a system limited to a one-week time frame. In our model the time frame was extended to 8 weeks, since bone formation is commonly assessed over a time frame of 8–12 weeks [5]. This allowed us to replicate four freshly created bone defects, with the ability to produce a rapid interaction and response to a variety of bone grafts. Similar models include an osteochondral model aimed at assessing cartilage repair developed by colleagues in our group [33], while another group recreated a necrotic bone defect environment to study bone repair [34–36]. However, since the osteochondral model contained both bone and cartilage tissues, its complex cellular cross-talks prevented analysis of the specific contribution of the bone fraction. In the second case, the bone construct did not replicate an osteoinductive bone microenvironment at the moment of implantation, the model required a complex surgery and was limited to one construct per animal. It is worth noting that in all these models, ours included, bone formation occurs in non-mechanically loaded environments, which are important factors during of skeletal regeneration [37]. However, all large bone defects in humans and animals require some kind of mechanical stabilisation/fixation in order for healing to take place. For this reason, our model best replicates these type of clinical situations.

In our model, constructs were created by sandwiching a bone ring between two PTFE caps, in order to create a core region only accessible for cells passing through the trabeculae of the bone ring. PTFE membranes are clinically used for alveolar ridge preservation [38], their biocompatibility is comparable to that of collagen membranes [39] and the beneficial effect on bone repair is mostly achieved by physically excluding unwanted connective tissue from the defect site. While we expect that this physical effect was key in producing a hypoxic bony microenvironment, depending on the scientific questions the absence of membranes or the use of alternative ones might allow to study different aspects relevant to bone regeneration, such as blood vessel attraction and invasion.

Vascularisation is a key event during bone formation. In the model for the necrotic bone mentioned above [34–36], angiogenesis was initiated in a comparable shaped devitalised bone ring construct by placing an arteriovenous bundle inside. The construct was then isolated from the surrounding tissues with a silicon-based membrane, causing vascularisation to occur from the inside outwards. However, the lack of peripheral vascularisation limited bone formation [34]. Since in our model the bone ring was not connected to the mouse blood supply at the moment of implantation, re-vascularisation occurred from the outside inwards, eventually reaching the whole volume of the construct. We thus hypothesised that the construct's core transiently accommodates a microenvironment with reduced oxygen, comparable to that present in a freshly-created bone defect. Studying the process and timing of revascularization and its possible implications for bone repair would be interesting for future experiments.

Due to the xenogeneic nature of the constructs, immunodeficient NMRI-*Foxn1* knock-out mice were used to prevent an immune rejection. These mice lack the T cell component, while maintaining the rest of immune system lineages. Although the T cell component plays a role in bone formation [40–42], our model unfortunately excludes this variable. On the other hand, these mice still possess macrophages and neutrophils, which allows several inflammatory processes relevant to callus formation during bone healing such as macrophage polarisation and their interaction with blood vessels to be studied [43–45].

To validate this new model, we tested several types of graft commonly used in the clinic and in small animal defect models. Clinically, the use of bone chips is the gold standard for the treatment of bone defects, thanks to their osteoinductive, osteoconductive and osteogenic properties. For this reason, a bone chip-based graft was first tested, and our observations of bone formation, bone resorption and

vascularisation, indicated active remodelling of the graft. Next, we tested a tissue engineered strategy in order to further validate the model. When chondrogenically differentiated MSC pellets were added, whose ability to undergo endochondral ossification is known to occur even in the absence of a bony environment [46], we observed that the pellets ossified as well as the regions within the defect between the pellets. This observation highlighted the ability of the ring to osseointegrate the graft contained inside independent of its shape. The collagen-based scaffolds used are known to ossify ectopically when harbouring chondrogenically differentiated MSCs [47]. However, when comparing the scaffolds, with and without cells, we observed that both scaffolds ossified to comparable levels, which matched the previous observation in rat calvarial defects [20,21]. Since the bone ring demonstrated the capability to initiate and sustain the ossification of its core, we further validated the model by assessing permissiveness to ossification of two grafts. On one hand, vital cartilage resisted calcification, as has been reported previously [48,49]. On the other hand and in line with the expected permissiveness to vascularisation described by Eisenstein et al. [23], the treated cartilage constructs permitted ossification as seen by the mineralised tissue, blood vessels and marrow formed inside. This observation further opens the possibility for our model to be used in studies that assess cartilage integrity. For all of this, we concluded that the bone microenvironment generated in the construct matches that of orthotopic *in vivo* models. Newer bone grafts formulations with improved properties are continuously being developed, based on natural and synthetic materials such as calcium phosphate-based fillings, bioactive glass, ceramics, or devitalised bone [50]. Thus, the semi-orthotopic bone presented here could be used to study and improve the osteogenic properties of those graft formulations such as cellular ingrowth capacity, stability and degradability, ability to osseointegrate or to induce bone formation.

5. Conclusion

In this study we conclude that the semi-orthotopic model developed recapitulates the graft-mediated healing response of a critical size bone defect, to a level accurate enough to make it suitable as a bone graft screening platform. Therefore, the model could be of interest in further experiments that study the interaction between the bone microenvironment and biomaterials (e.g., metal implants, a variety of scaffolds), which may contain bioactive substances (e.g., growth factors, drugs or small molecules including genetic cargos) and/or cells (stromal cells, osteoblasts, etc.). Although we focused on the main outcome of bone formation of our model, further uses could be extended to situations where the cellular interactions with a bone microenvironment are key, as in the case of bone tumours. In addition, future modifications of the model may consider including micro-CT-based quantitative measurements of vascularisation, even in combination with mouse reporter strains.

Declaration of competing interest

The authors declare that they have no known competing financial interests or personal relationships that could have appeared to influence the work reported in this paper.

Acknowledgements

This project has received funding from the European Union's Horizon 2020 research and innovation program under Marie Sklodowska-Curie grant agreement no. 721432. This work was performed within the framework of the Erasmus Postgraduate School Molecular Medicine and Medical Delta Regenerative Medicine 4D program. This work was supported through the use of imaging equipment provided by the Applied Molecular Imaging Erasmus University Medical Center facility.

Appendix A. Supplementary data

Supplementary data to this article can be found online at https://doi.org/10.1016/j.biomaterials.2021.121187.

Author contributions

E. Andrés Sastre: Conceptualization, Supervision, Formal analysis, Investigation, Writing - Original Draft, Visualization. **Y. Nossin**: Investigation, Writing - Review & Editing. **I. Jansen**: Formal analysis, Investigation, Writing - Review & Editing, Visualization. **N. Kops**: Investigation, Writing - Review & Editing. **C. Intini**: Resources, Writing - Review & Editing. **J. Witte-Bouma**: Investigation, Writing - Review & Editing. **B. van Rietbergen**: Formal analysis, Writing - Review & Editing. **S. Hofmann**: Conceptualization, Writing - Review & Editing. **Y. Ridwan**: Resources, Writing - Review & Editing. **J.P. Gleeson**: Resources, Writing - Review & Editing. **F.J. O'Brien**: Resources, Writing - Review & Editing. **E.B. Wolvius**: Resources, Writing - Review & Editing. **G.J.V.M. van Osch**: Conceptualization, Supervision, Funding acquisition, Writing - Review & Editing. **E. Farrell**: Conceptualization, Supervision, Funding acquisition, Writing - Review & Editing.

Data availability

The raw data required to reproduce these findings are available upon request. The scripts used for the image analyses are available upon request. The processed data required to reproduce these findings are available upon request.

References

[1] R. Dimitriou, et al., Bone regeneration: current concepts and future directions, BMC Med. 9 (2011) 66.
[2] T.T. Roberts, A.J. Rosenbaum, Bone grafts, bone substitutes and orthobiologics: the bridge between basic science and clinical advancements in fracture healing, Organogenesis 8 (4) (2012) 114–124.
[3] A. Ho-Shui-Ling, et al., Bone regeneration strategies: engineered scaffolds, bioactive molecules and stem cells current stage and future perspectives, Biomaterials 180 (2018) 143–162.
[4] S. Ehnert, et al., Use of in vitro bone models to screen for altered bone metabolism, osteopathies, and fracture healing: challenges of complex models, Arch. Toxicol. 94 (12) (2020) 3937–3958.
[5] M.A. Scott, et al., Brief review of models of ectopic bone formation, Stem Cell. Dev. 21 (5) (2012) 655–667.
[6] A. Schindeler, et al., Preclinical models for orthopedic research and bone tissue engineering, J. Orthop. Res. 36 (3) (2018) 832–840.
[7] J. Chalmers, D.H. Gray, J. Rush, Observations on the induction of bone in soft tissues, J. Bone Jt. Surg. Br. Vol. 57-B (1) (1975) 36–45.
[8] M.L. de Vries-van Melle, et al., An osteochondral culture model to study mechanisms involved in articular cartilage repair, Tissue Eng. C Methods 18 (1) (2012) 45–53.
[9] D. Zaffe, F. D'Avenia, A novel bone scraper for intraoral harvesting: a device for filling small bone defects, Clin. Oral Implants Res. 18 (4) (2007) 525–533.
[10] C.A. Knuth, et al., Isolating pediatric mesenchymal stem cells with enhanced expansion and differentiation capabilities, Tissue Eng. C Methods 24 (6) (2018) 313–321.
[11] F. O'Brien, Influence of freezing rate on pore structure in freeze-dried collagen-GAG scaffolds, Biomaterials 25 (6) (2004) 1077–1086.
[12] A. Lolli, et al., Silencing of antichondrogenic MicroRNA-221 in human mesenchymal stem cells promotes cartilage repair in vivo, Stem Cell. 34 (7) (2016) 1801–1811.
[13] A. Lolli, et al., Hydrogel-based delivery of antimiR-221 enhances cartilage regeneration by endogenous cells, J. Contr. Release 309 (2019) 220–230.
[14] M.L. Vainieri, et al., Evaluation of biomimetic hyaluronic-based hydrogels with enhanced endogenous cell recruitment and cartilage matrix formation, Acta Biomater. 101 (2020) 293–303.
[15] P. Christen, R. Muller, In vivo visualisation and quantification of bone resorption and bone formation from time-lapse imaging, Curr. Osteoporos. Rep. 15 (4) (2017) 311–317.
[16] J.H. Waarsing, et al., Detecting and tracking local changes in the tibiae of individual rats: a novel method to analyse longitudinal in vivo micro-CT data, Bone 34 (1) (2004) 163–169.
[17] F. Gaytan, et al., A novel RGB-trichrome staining method for routine histological analysis of musculoskeletal tissues, Sci. Rep. 10 (1) (2020) 16659.
[18] J. Sedgewick, Acquisition and post-processing of immunohistochemical images, Methods Mol. Biol. 1554 (2017) 75–106.

[19] B. Johnstone, et al., In vitro chondrogenesis of bone marrow-derived mesenchymal progenitor cells, Exp. Cell Res. 238 (1) (1998) 265–272.
[20] M. Alhag, et al., Evaluation of the ability of collagen-glycosaminoglycan scaffolds with or without mesenchymal stem cells to heal bone defects in Wistar rats, Oral Maxillofac. Surg. 16 (1) (2012) 47–55.
[21] F.G. Lyons, et al., The healing of bony defects by cell-free collagen-based scaffolds compared to stem cell-seeded tissue engineered constructs, Biomaterials 31 (35) (2010) 9232–9243.
[22] E.M. Thompson, et al., An endochondral ossification-based approach to bone repair: chondrogenically primed mesenchymal stem cell-laden scaffolds support greater repair of critical-sized cranial defects than osteogenically stimulated constructs in vivo, Tissue Eng. 22 (5–6) (2016) 556–567.
[23] K.K. Sorgente N, L.W. Soble, R. Eisenstein, The resistance of certain tissues to invasion. II. Evidence for extractable factors in cartilage which inhibit invasion by vascularized mesenchyme, Lab. Invest. 32 (1975) 217–222.
[24] R.C. Hubrecht, E. Carter, The 3Rs and humane experimental technique: implementing change, Animals (Basel) 9 (10) (2019).
[25] M. Haffner-Luntzer, et al., Mouse models in bone fracture healing research, Current Molecular Biology Reports 2 (2) (2016) 101–111.
[26] S. Zwingenberger, et al., Establishment of a femoral critical-size bone defect model in immunodeficient mice, J. Surg. Res. 181 (1) (2013) e7–e14.
[27] X. Yu, et al., Controlling the structural organization of regenerated bone by tailoring tissue engineering scaffold architecture, J. Mater. Chem. 22 (19) (2012).
[28] O. Gauthier, et al., In vivo bone regeneration with injectable calcium phosphate biomaterial: a three-dimensional micro-computed tomographic, biomechanical and SEM study, Biomaterials 26 (27) (2005) 5444–5453.
[29] H.W. Kim, et al., Bone formation on the apatite-coated zirconia porous scaffolds within a rabbit calvarial defect, J. Biomater. Appl. 22 (6) (2008) 485–504.
[30] E.H. Lee, et al., A combination graft of low-molecular-weight silk fibroin with Choukroun platelet-rich fibrin for rabbit calvarial defect, Oral Surg. Oral Med. Oral Pathol. Oral Radiol. Endod. 109 (5) (2010) e33–e38.
[31] X.L. Wang, et al., Exogenous phytoestrogenic molecule icaritin incorporated into a porous scaffold for enhancing bone defect repair, J. Orthop. Res. 31 (1) (2013) 164–172.
[32] I. Moreno-Jimenez, et al., The chorioallantoic membrane (CAM) assay for the study of human bone regeneration: a refinement animal model for tissue engineering, Sci. Rep. 6 (2016) 32168.
[33] M.L. de Vries–van Melle, et al., Chondrogenesis of mesenchymal stem cells in an osteochondral environment is mediated by the subchondral bone, Tissue Eng. 20 (1–2) (2014) 23–33.
[34] C. Epple, et al., Prefabrication of a large pedicled bone graft by engineering the germ for de novo vascularization and osteoinduction, Biomaterials 192 (2019) 118–127.
[35] T. Ismail, et al., Engineered, axially-vascularized osteogenic grafts from human adipose-derived cells to treat avascular necrosis of bone in a rat model, Acta Biomater. 63 (2017) 236–245.
[36] T. Ismail, et al., Platelet-rich plasma and stromal vascular fraction cells for the engineering of axially vascularized osteogenic grafts, J Tissue Eng Regen Med 14 (12) (2020) 1908–1917.
[37] D.C. Betts, R. Muller, Mechanical regulation of bone regeneration: theories, models, and experiments, Front. Endocrinol. 5 (2014) 211.
[38] P. Papi, et al., The use of a non-absorbable membrane as an occlusive barrier for alveolar ridge preservation: a one year follow-up prospective cohort study, Antibiotics (Basel) 9 (3) (2020).
[39] T. Korzinskas, et al., In vivo analysis of the biocompatibility and macrophage response of a non-resorbable PTFE membrane for guided bone regeneration, Int. J. Mol. Sci. 19 (10) (2018).
[40] G. Mori, et al., The Interplay between the bone and the immune system, Clin. Dev. Immunol. 2013 (2013) 720504.
[41] C. Schlundt, et al., Individual effector/regulator T cell ratios impact bone regeneration, Front. Immunol. 10 (2019) 1954.
[42] T. El Khassawna, et al., T lymphocytes influence the mineralization process of bone, Front. Immunol. 8 (2017) 562.
[43] C. Schlundt, et al., The multifaceted roles of macrophages in bone regeneration: a story of polarization, activation and time, Acta Biomater. 133 (2021) 46–57.
[44] J. Stefanowski, et al., Spatial distribution of macrophages during callus formation and maturation reveals close crosstalk between macrophages and newly forming vessels, Front. Immunol. 10 (2019) 2588.
[45] C. Schlundt, et al., Macrophages in bone fracture healing: their essential role in endochondral ossification, Bone 106 (2018) 78–89.
[46] C. Knuth, et al., Understanding tissue-engineered endochondral ossification; towards improved bone formation, Eur. Cell. Mater. 37 (2019) 277–291.
[47] E. Farrell, et al., In-vivo generation of bone via endochondral ossification by in-vitro chondrogenic priming of adult human and rat mesenchymal stem cells, BMC Muscoskel. Disord. 12 (2011) 31.
[48] S.H. Jo, et al., Tracheal calcification, CMAJ (Can. Med. Assoc. J.) 179 (3) (2008) 291.
[49] H. Claassen, et al., Different patterns of cartilage mineralization analyzed by comparison of human, porcine, and bovine laryngeal cartilages, J. Histochem. Cytochem. 65 (6) (2017) 367–379.
[50] M.M. Stevens, Biomaterials for bone tissue engineering, Mater. Today 11 (5) (2008) 18–25.